Chem Soc Rev

Imaging of β-amyloid plaques by near infrared fluorescent tracers: A new frontier for chemical neuroscience

Journal:	*Chemical Society Reviews*
Manuscript ID:	CS-TRV-10-2014-000337.R1
Article Type:	Tutorial Review
Date Submitted by the Author:	10-Oct-2014
Complete List of Authors:	Staderini, Matteo; Universidad Complutense, Facultad de Farmacia, Química Orgánica y Farmacéutica Martín, M. Antonia; Universidad Complutense, Sección Departamental de Química Analítica Bolognesi, Maria Laura; Università di Bologna, Dipartimento di Scienze Farmaceutiche Menendez, J. Carlos; Universidad Complutense, Quimica Organica y Farmaceutica

Journal Name

RSCPublishing

ARTICLE

Imaging of β-amyloid plaques by near infrared fluorescent tracers: A new frontier for chemical neuroscience

Cite this: DOI: 10.1039/x0xx00000x

Received ooth January 2012,
Accepted ooth January 2012

DOI: 10.1039/x0xx00000x

www.rsc.org/

Matteo Staderini,[a] María Antonia Martín,[b] Maria Laura Bolognesi[c] and J. Carlos Menéndez[a]*

Brain amyloid depositions are the main hallmark of Alzheimer's and other protein misfolding diseases. Since they are believed to precede clinical symptoms by several years, imaging of such fibrillar aggregates is particularly suitable to diagnose the onset of the disease in its early stage and monitor its progression. In this context, near infrared (NIR) imaging has been proposed as a promising and non-invasive method to visualize amyloid plaques *in vivo* because of its acceptable depth of penetration and minimal degree of tissue damage. In this tutorial review, we describe the main chemical and physicochemical features of probes associated to fluorescence emission in the NIR region. The review focuses on the recent progresses and improvements in the development of small-molecule NIR fluorescent probes and their *in vivo* application in living animals. In addition, the possible therapeutic application of NIR probes to block the pathological aggregation process will be discussed, raising the fascinating possibility of their exploitation as theranostic agents.

1. Introduction

In the last decades protein misfolding diseases (PMD), characterized by the structural change of normally expressed proteins to amyloidogenic conformations, have come to public and scientific attention due to the fact that they are increasing enormously in developed countries and becoming a serious problem in terms of health and economic costs.[1] Alzheimer's disease (AD), prion diseases (PrDs), Parkinson's disease (PD) and amyotrophic lateral sclerosis are prominent examples of PMDs, in which the misfolded proteins trigger the degeneration of brain tissue. Among them, AD is the most common type of dementia characterized by a progressive cognitive decline and loss of the ability to learn, reason and communicate. One of the main hallmarks of AD is the formation and accumulation of proteinaceous aggregates known as β-amyloid (Aβ) plaques. These amyloidogenic deposits consist mainly of two peptides, $A\beta_{40}$ and $A\beta_{42}$, resulting from the proteolytic cleavage of the transmembrane glycoprotein amyloid precursor protein (APP). Aβ peptides are rich in β-sheet secondary structures, which are insoluble and resistant to proteolytic digestion and tend to aggregate in plaques. Although plaques have long been associated with the diseases, the soluble oligomeric forms represent the toxic species leading to neuronal death and to the disruption of memory.[2]

Despite numerous efforts and an exponential growth in investment, treatments able to definitely arrest the course of this disease do not exist to date. The lack of effective drugs in the market is due to the fact that the aetiology of AD is not well understood and consequently no therapeutic targets have been validated. Another important motive for the high attrition of drugs in the clinic is related to the poor predictive power of animal models for efficacy in humans.[3] Furthermore, the failure of many drug candidates has been attributed to their administration at a late stage, when the pathology is too advanced. On these bases, the development of proper biomarkers for early diagnosis and disease monitoring appears to be critical for an efficacious therapy. In this context, it is relevant to note that Aβ depositions are believed to precede clinical symptoms by several years.[4] Consequently, *in vivo* imaging of Aβ is particularly suitable for identifying individuals at risk and in the early stages of AD.

Congo Red (CR), thioflavin T (ThT) and other dyes are widely used for post-mortem AD diagnosis through the histological stain of amyloid fibrils and in the evaluation of PET ligands. Through the years, great strides forward have been made in the field of molecular imaging with the aim of detecting abnormal proteinaceous deposits *in vivo*. Generally speaking, MRI (magnetic resonance imaging) and PET (positron emission tomography) are the most used imaging

techniques in clinical settings. However, MRI has too low a sensitivity for amyloid imaging, and PET has some serious limitations due to its high cost, the scarcity of the required isotopes and practical limitations in their use associated to the need to prepare and use them within the short half-lives of the radioactive atomic species (20 min in the case of ^{14}C and 110 min for ^{18}F).[5] In addition, PET has not found practical application for monitoring drug effectiveness in mice because of the complexity of the experimental procedure and data analysis protocols required for small animals. On the other hand, fluorescence spectroscopy has proven suitable for studying fibrillar aggregates.

There is a growing interest in fluorescence spectroscopy as a non-invasive alternative for early diagnosis that enables the real-time visualization of biomolecules in living systems. It is a versatile and sensitive method that leads to a rapid, inexpensive and non-radioactive imaging system.[5] It is important to remark that for their potential *in vivo* application, fluorescent probes have to possess proper features including the ability to emit fluorescence in the far-red or near-infrared (NIR) region (600-900 nm). In fact, NIR light is particularly suitable to be used for *in vivo* imaging of molecular processes due its acceptable depth of penetration, non-invasive operation, minimal interferences from auto-fluorescence of biological matter and minimal photo-damage to biological samples.[6] Furthermore, in this spectral range the absorption of fluorescence signals by body tissues are minimal. Recent studies indicate that the NIR-IIa window (1300-1400 nm) is particularly promising in this regard because the scattering coefficient of brain tissue is particularly low in this region (2.54 mm^{-1} at 1350 nm *vs.* 7.49 mm^{-1} at 800 nm), although the exploration of this possibility has barely begun.[7]

So far, NIR fluorescent probes have been mainly used in the oncology field for imaging tumours, both *in vivo* and *in vitro*. They are also extremely useful to visualize and monitor Aβ plaque formation and to evaluate the effectiveness of drug treatment in animal models and they are therefore considered an attractive and promising diagnostic tool for AD. Nevertheless, a note of caution is needed in this regard since correlation between AD status and amyloid accumulation is weak and these biomarkers are currently limited to monitor progress in individuals, providing only good negative AD diagnosis.[8] AD PET probes have found the same limitations, and they are regarded as being able to rule out AD, but not confirm it.

To our knowledge, very few reviews are available about the design strategies and bioimaging applications of NIR sensors, and they only cover the literature up to 2010.[9,10,11,12] Recently, Guo and coworkers published a review on the advances made in the development and use of NIR fluorescent probes for tracing important intracellular species such as reactive oxygen species (ROS) and reactive nitrogen species (RNS), metal ions and anions, enzymes and other related species, as well as intracellular pH changes, without mentioning Aβ plaques.[13] Another review by Lin *et al.* is focused on improvements related to physicochemical properties of NIR probes, classifying them into different categories according to their organic structure.[14] However, none of these existing reviews cover the imaging of fibrillar aggregates by NIR techniques.

The application of NIR imaging in neurodegenerative diseases is challenging due to the fact that Aβ plaques are located into the skull-shielded brain. Indeed, fluorescence-based optical imaging of the brain of small animals in traditional near-infrared regions has previously relied on craniotomy, cranial windows and skull-thinning techniques. Since the resolution of optical imaging decreases with increasing depth of the source of fluorescence emission because of fluorescence scattering in the biological environment, quantification of the amyloid load by NIR imaging is limited to the surface area of the brain.

The development of modern and efficient optical imaging systems such as fluorescent molecular tomographic (FMT) imaging and the hybrid technique known as FMT-CT (X-ray computed tomography) imaging have enabled the *in vivo* visualization of Aβ plaque distribution in AD mice with an intact cranium. Nevertheless, mice do not develop the same neuropathological or clinical characteristics seen in humans, and therefore amyloid aggregates in transgenic mouse models are different to those observed in AD patients, thereby hampering the translation into clinics of diagnostic or therapeutic findings done in these models.[3] Although further technological improvements are needed and it is not likely that the entire human brain can be visualized using optical methods, it has been proposed that it will be feasible in the near future to probe the brain cortex at depths up to 3–5 cm.[15] This should be sufficient for obtaining diagnostic information on AD patients, taking into account that most of the amyloid depositions are placed on the neo-cortical surface, although the problem of non-specific binding to white matter has to be taken into account.[16]

Another possible approach to NIR AD imaging could be based on the use of parts of the central nervous system (CNS) that are not shielded by the skull and can therefore be considered physiological skull windows. For instance, the retina, which is easily accessible for direct and non-invasive imaging, could provide a unique opportunity for early diagnosis of AD in animal models and humans by exploiting NIR imaging. Thus, recent findings demonstrated the presence of Aβ plaques in the retina, of AD patients with similar biochemical properties of those observed in their brains,[17] and curcumin was shown to bind these plaques and allow their visualization *in vivo* at high resolution.[17] Unfortunately, Schon *et al.* could not find any evidence for the presence of Aβ plaques in retina of transgenic mice or AD patients, challenging the results of the previous work.[18] On the other hand, they were able to detect fibrillar tau aggregates *in vivo* in transgenic mice retina, whereas only hyperphosphorylated (but not fibrillar) tau was observed in AD human retina.[18] The olfactory epithelium, being also an extension of the brain, can be viewed as an optimum target for NIR imaging. It is interesting to note that the presence of neurofibrillary tangles was confirmed by staining, whereas no Aβ deposits could be observed in this region.[19]

In this review we will focus on small-molecule NIR probes used to image amyloidogenic deposits *in vivo*, highlighting the most recent progress toward the evaluation of new sensors with enhanced spectroscopic and physicochemical properties. In addition, the possible therapeutic application of NIR probes to block the pathological aggregation process will be discussed.[4] In biomedicine, a theranostic agent is described as one endowed with both therapeutic and diagnostic features.[20,21] The principles governing the design of theranostic agents against neurodegenerative diseases based on NIR emission will also be discussed.

2. NIR fluorescent probes

There are two potential approaches to NIR imaging involving the use of fluorescence emission nanoparticles (quantum dots) or *in vivo* imaging tracers. The former present advantageous spectroscopic properties compared to organic fluorophores, since they show narrower emission spectra without tailing at longer wavelengths and they have a high Stokes' shift. In the context of this review, changes in the state of aggregation of amyloid fibrils in the presence of NPs presenting a core of CdSe and a shell of ZnS have been demonstrated.[22] Similarly, single-wall carbon nanotubes containing a fluorescent sensor (IRDye800) have been proposed for the fluorescence imaging of mouse cerebral vasculature without craniotomy.[7] Nevertheless, quantum dots and carbon nanotubes pose a number of health risks, even at very low concentrations, including cell damage, cell apoptosis and alterations in renal function.[23] The rest of this review will be focused on small molecule tracers.

Since the discovery of amyloid depositions more than a century ago, several fluorescent dyes with high affinity for the amyloid species have been generated for the *post-mortem* diagnosis of AD and other PMDs.[24] Nevertheless, most conventional dyes cannot translate into clinical diagnostic tools because of their low specificity, poor sensitivity, inability to cross the blood brain barrier (BBB) and marked toxicity. Many efforts have been done to overcome these drawbacks with the purpose of obtaining an optical marker to be used for *in vivo* imaging of Aβ plaques. To this end, NIR probes have been proposed as ideal candidates. Apart from the ability to emit fluorescence in the NIR region,[6] these probes must possess additional features including: (1) specificity to Aβ plaques, (2) ability to change fluorescence properties upon binding to fibrils, (3) high-affinity binding, (4) high fluorescence quantum yield, (5) large Stokes shift, (6) minimum interference from human serum albumin (HSA) binding, (7) small molecular size and a suitable lipophilicity, enabling the molecule to cross the BBB, and (8) low toxicity.[25,26]

2.1 Molecular design for emission in the NIR region

If the suitable amount of energy is given to a molecule, electrons can be promoted from an occupied, low-energy molecular orbital to an empty, higher-energy one, giving rise to a transition that corresponds to an absorption band in the spectrum. For a large number of organic compounds, energy is then dissipated by collision with solvent molecules. In the case of fluorescent compounds, electrons from the excited state return to the ground state by emission of photons, the latter phenomenon being known as fluorescence, because the electrons of the excited and ground states are paired (singlet state). The smallest possible difference in energy between a full and an empty orbital is the one existing between the highest occupied molecular orbital (HOMO) and lowest unoccupied molecular orbital (LUMO), called the HOMO-LUMO gap, which is closely correlated to the absorption and emission wavelengths. In fact, for a low energy gap a red shift in absorption and emission spectra would be expected. In line with these considerations, NIR probes have been designed with the aim of reducing the HOMO-LUMO gap of existing amyloid dyes. This can be achieved by extended conjugation, and therefore conjugated π systems are ideal scaffolds for the construction of NIR probes and a change of the conjugation length represents an effective way to tune the energy gap level. However, achieving NIR emission by conjugation alone would require the construction of prohibitively big molecules. A very common strategy used to lower the HOMO-LUMO gap of a conjugated π system is based upon the presence of electron-donor (D) and electron-acceptor (A) groups as terminal moieties in order to generate a "push-pull molecule". In its ground state, such a D-A molecule can be described by two resonance forms, one of which is neutral and the other one is zwitterionic (Figure 1), with the latter form being a better representation of the excited state. Due to the presence of the A and D groups, the whole conjugated system is more polarized and, in terms of energy, the ground state is closer to the excited state. Therefore, less energy is needed for the absorption and emission transitions and thus a bathochromic shift is observed. It is important to remark that obtaining the desired shift depends on the electronic features of D and A. The electron donor group must possess a lone pair of electrons in a π orbital able to interact with the π-molecular orbitals of the conjugated system increasing the HOMO energy. On the other hand, the LUMO orbitals are made more stable by the interaction with the antibonding orbitals of the π electron-withdrawing group. Both concomitant effects lead to reduction of the HOMO-LUMO gap. Among the π-electron donor groups, dimethylamino (NMe_2) is widely regarded as the best red-shift absorption-pushing group, whereas the formyl and cyano moieties are considered optimum acceptors. Moreover, pH can also influence the bathochromic shift of push-pull molecules. In a medium with pH around 7 the neutral form is generally dominant, often showing short absorption/emission wavelengths due to the weak push-pull system. In acidic conditions, an ionic form having a strong push-pull system become dominant and a red shift in absorption/emission is observed.[27]

A donor-acceptor-donor (D-A-D) architecture is preferred when two photon microscopy (TPM) bioimaging is applied.[28]

TPM has some advantages compared to one photon microscopy including increased depth penetration by exciting at a longer wavelength, enhanced 3D resolution and reduced photodamage. Unfortunately, the technique is invasive *in vivo* and cannot be used in the clinic.[29] TPM features a nonlinear dependence between absorbed light and incident light intensity, since in two-photon absorption (TPA) processes two photons are absorbed with a probability that is proportional to the square of the incident light intensity.[28] Considering that TPA efficiency depends on the conjugation length and D/A strength, a D-A-D system furnishes higher TPA cross sections (a measure for the probability of an absorption process) than a D-A molecule.[28]

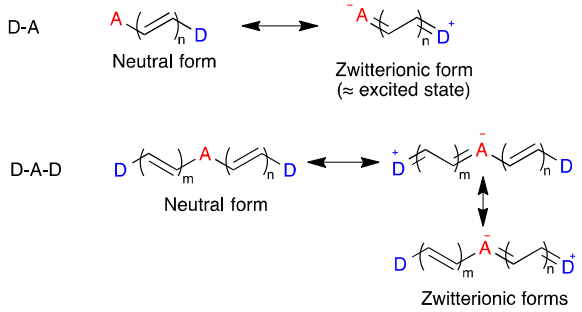

Fig. 1 A push-pull molecule and a donor-acceptor-donor molecule, showing their neutral and zwitterionic forms.

Another important factor that must be considered for the reduction of the energy gap is the bond length alternation (BLA). BLA is the length difference between consecutive single and double bonds and its value quantifies the delocalization of electrons across the whole molecule. In fact, in a conjugated system a single C-C bond has a partial double bond character due to the overlap of the π orbitals, and hence its length is slightly shorter than a standard single bond (154 pm) and closer to a double one (134 pm). Furthermore, because of this overlap it becomes harder to rotate this "formal single bond" and the molecular structure tend to adopt a planar conformation. Based on these considerations, if the BLA is close to zero it means that there is a great overlap among the π orbitals and consequently the system is highly conjugated and the electrons very delocalized, leading to a reduction of the HOMO-LUMO gap. In push-pull molecules, the presence of D and A leads to an increase of the double-bond character of the C-C bonds, resulting in a reduction of the BLA value as well as the energy gap.

As mentioned above, π orbitals overlap and combine better if the molecule is planar. In this way, a big molecular orbital over the whole molecule is generated that allows a strong π conjugation and a great delocalization of the electrons. This effect explains why the fluorescent emission maximum of compounds in their solid state is observed at longer wavelengths with regard to those obtained in solution. Indeed, in the solid state the free movements of a molecule are restricted resulting in a more rigid conformation, whereas in solution it possesses a substantial degree of conformational freedom. Planarity is a common structural feature of fluorescent molecules, but it is not a requirement, and excited states have been proved to be non-planar in some cases, such as thioflavin T.[30] In the case of molecules containing aromatic rings linked by ethylene chains, which is the most common structure for amyloid probes, a change in the geometry of the molecule from the ground to the excited state is accompanied by a red shift in the fluorescent emission, together with a broadening of the spectrum. Furthermore, the donor-acceptor energy transfer effects may be enhanced by such changes in the excited state geometry.

Upon binding to aggregate β-amyloid proteins, fluorescent probes normally show shifts of their emission maxima and an increase in the fluorescent quantum yield. These effects are similar to those found upon an increase of viscosity of the medium and are due to conformational changes, since when the molecule is in unbound condition, *e.g.* in solution, free rotation around the single bonds is allowed, whereas upon binding to fibrils, where these movements are restricted and its rings are held rigidly, it becomes more planar, triggering a change in the HOMO-LUMO gap and a concomitant shift in the absorption maximum. In addition, in such a rigid system the vibrational-rotational processes that couple the excited and the ground state are reduced and therefore the radiationless decay rate decreases, giving rise to an enhancement of the fluorescent yield. As previously mentioned, fluorescence quantum yield enhancement upon binding to fibrils is a desirable feature for a probe, in order for its fluorescence to be clearly distinguished from that of the background.

In summary, different factors influence the π* → π transition reducing the energy gap between HOMO-LUMO including the extension of the conjugated system, the introduction of electron donor and acceptor moieties, the bond length alternation and the degree of planarity. Building on this knowledge, several fluorescent NIR probes have been designed to stain amyloid plaques.

2.2 NIR probes imaging amyloid plaques *in vivo*

2.2.1. NIAD-4 and related compounds

NIAD-4 (**1**) is considered a milestone, as it was one of the first NIR probes used to image β-amyloid plaques *in vivo*.[25] NIAD-4 was designed by merging the chemical features of CR and ThT, as well as considering all the points outlined in the previous chapter to generate a biomarker able to emit fluorescence in the NIR region. It presents the classical push-pull architecture in which a *p*-hydroxyphenyl group (D) and a dicyanomethylene group (A) are connected by a dithienylethenyl π-conjugated bridge making the whole molecule highly polarizable. The introduction of an aromatic π system was dictated by the fact that it can provide hydrophobic interactions to bind the surface of the amyloid fibrils. It is interesting to note that compound **1** changes its fluorescent properties upon binding to fibrils. Indeed, in the presence of synthetic aggregated β-amyloid proteins, the dye showed a noteworthy red shift (absorption above 600 nm) and the binding

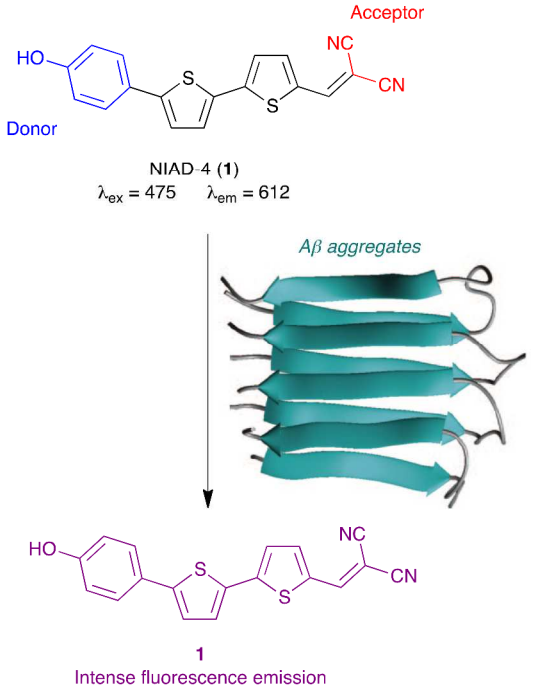

Fig.2 The push-pull architecture of NIAD-4 (**1**). A strong enhancement of the fluorescent signal is observed when **1** binds the Aβ fibrillar aggregates.

was accompanied by a strong enhancement (400 fold) of the fluorescent intensity (Figure 2). The potential of NIAD-4 as an amyloid sensor was first assessed by a binding study *in vitro*. Its binding constant, evaluated from competition binding assays, was in the two-digit nanomolar range (K_i = 10 nM), showing that NIAD-4 has a much higher affinity than ThT (K_i = 580 nM). Finally, the dye was tested *in vivo* in transgenic AD mice with a cranial window to allow direct monitoring of the brain surface by multiphoton microscopy. The biomarker turned out to be able to cross the blood brain barrier (BBB) after intravenous injection and bound with high specificity to Aβ plaques in the living brain, allowing their easy detection due to its intense red fluorescence. This specific binding was then confirmed *ex-vivo*, by the histopathological studies on the brain slices of the sacrificed mice.

Despite the high labeling specificity of **1** for Aβ plaques, its emission wavelength falls just in the NIR region and the imaging method used was invasive. To this respect, new NIR smart probes with improved optical properties coupled with advanced and less invasive technologies were needed. With this in mind, the same authors developed two NIAD-4 derivatives termed NIAD-11 (**2**) and NIAD-16 (**3**) that showed enhanced spectral characteristics as well as quantum efficiency (Fig. 3).[31] Compound **2** bears an additional hydroxyl group in the phenyl fragment to reinforce the pushing effect, connected to a benzo-thienyl ring instead of thiophene. This dye upon binding to fibrils showed a considerable fluorescent quantum yield 10 fold superior than the unbound form, together with an exceptional emission maximum above 700 nm. Compound **3** was obtained by replacing the terminal hydroxyl group of NIAD-4 with a dimethylamino group that resulted in a bathochromic shift of the emission maximum (λ_{em} = 720 nm).

2.2.2. Methoxy-X04 and polythiophenes

In an effort to overcome the drawbacks encountered by

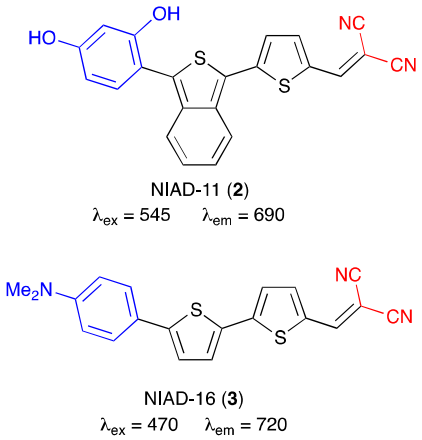

Fig.3 Chemical modification of NIAD-4 gave rise to the second-generation compounds NIAD-11 (**2**) and NIAD-16 (**3**), with improved optical features.

conventional dyes, a CR derivative, named methoxy-X04 (**4**) (Fig. 4), was designed with a lower molecular weight, increased lipophilic character and uncharged to provide a much higher brain permeation than its predecessor.[32] Methoxy-X04 has nanomolar affinity to fibrillar aggregates *in vitro* and selectively binds Aβ plaques in brain slices of AD patients. Due to its fluorescence, it was injected into transgenic mice that overexpressed amyloid lesions and imaged by TPM on open skull. The biomarker could distinguish amyloid depositions at high resolution, as confirmed by *ex vivo* analysis.

Although not structurally related, we will now mention luminescent conjugated polythiophenes (LCPs) because they were also evaluated for their use in optical imaging of amyloid deposits by multiphoton spectroscopy.[33] LCPs exploit their conjugated polymer backbones to emit fluorescence with high quantum efficiency. For instance, in the case of PTAA (polythiophene acetic acid, **5**) (Fig. 4), different emission spectra were observed depending on the conformation of the protein. PTAA, due to the planar conformation that adopts when binding to amyloid fibrils, emits a strong orange-red light (λ_{em} = 590 nm) allowing the detection and discrimination of amyloid deposits from the rest of brain tissue of AD patients (blue autofluorescence) observed by confocal microscopy.[33] Aβ plaques were also visualized *in vitro* with this biomarker by

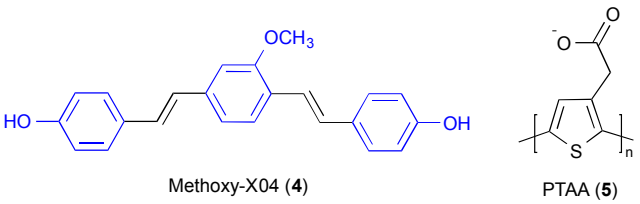

Fig.4 Structures of methoxy-X04 and PTAA

using TPM upon excitation at 820 nm, with high sensitivity and contrast between the signals from the amyloid deposits and the surrounding tissue.

2.2.3. Boron dipyrromethane (BODIPY)-based fluorescent probes

In search for novel NIR probes, Ono *et al.* focused on the boron dipyrromethane (BODIPY) moiety, since it constitutes the scaffold of many dyes used for biological applications.[34] They combined the BODIPY fragment with a portion of NIAD-4 (2-phenylthiophene), obtaining an extended conjugated system that they called BODIPY7 (**6**) (Fig. 5a).[35] This derivative showed a high affinity for Aβ aggregates (K_i = 108 nM) *in vitro* and stained selectively amyloid plaques in brain tissue sections of AD transgenic mice.

Regarding its optical features, compound **6** displayed a high fluorescent quantum yield and an absorption/emission wavelength at 606 and 613 nm, just in the NIR range. Nonetheless, the low brain uptake of BODIBY7 did not allow its application *in vivo*, thereby it was modified to overcome this limit and to further red-shift its absorption/emission maximum. A new BODIPY-based probe was generated (BAP-1, **7**) employing a classical push-pull architecture where a BODIPY unit, which represents the acceptor, was connected to a dimethylamino styryl group, the donor.[36] As expected the new probe absorbed and emitted light in the NIR region (604/648 nm) accompanied by a high fluorescent quantum yield. In addition, compound **7** confirmed very high affinity for Aβ aggregates (K_i = 44.1 nM) *in vitro*. Furthermore, *ex vivo* experiments were carried out in order to prove the ability of **7** to cross the BBB and selectively label amyloid fibrils. Transgenic mice (Tg2576) that overexpress Aβ plaques were used, as well as wild type mice as control After injection of **7** into the two types of mice, higher fluorescent signals were observed on the brain of the Tg2576 mice than that of the control ones (Fig. 5b). Despite the high binding affinity to amyloid fibrils, compound **7** did not meet the ideal requirements to be used *in vivo* due to its nonspecific accumulation in the scalp.

Starting from these results, the chemical structure of **7** was modified with the aim of obtaining higher resolution imaging of Aβ plaques *in vivo*. Replacing the phenyl group with a thiophenyl or furanyl group, four novel BODIPY derivatives (BAP 2-5, **8-11**) were generated (Fig. 6).[37] All the compounds exhibited longer absorption and emission wavelengths maintaining high affinity and selectivity for Aβ aggregates *in vitro*. Since biodistribution experiments showed that compound BAP-2 (**8**) had good uptake into and fast washout from the brain, it was selected as a candidate for NIR imaging *in vivo*. This probe was injected into transgenic mice that overexpressed Aβ plaques. After two hours, the analysis of the mice brain section revealed that compound **8** penetrated the BBB and selectively bound the fibrils. On the other hand, *in vivo* imaging

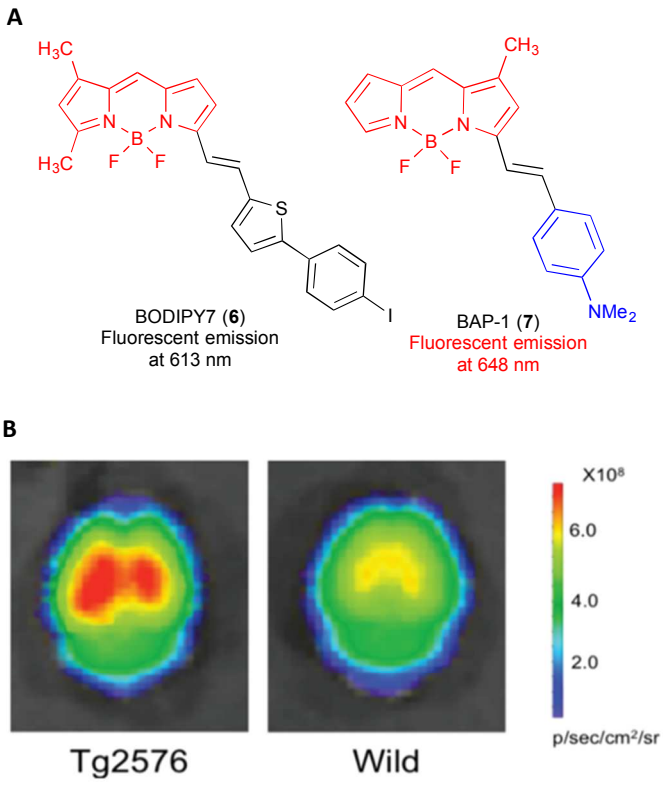

Fig. 5 (A) BODIPY7 (**6**) was modified by introducing a donor group in order to produce an efficient push-pull system (BAP-1, **7**), thereby red-shifting the fluorescence emission. (B) Fluorescent intensity signals were higher from the brain of the Tg2576 mice compared with that from the wild type mice after injection of **7**. Adapted with permission from M. Ono, H. Watanabe, H. Kimura and H. Saji, *ACS Chem. Neurosci.*, 2012, **3**, 319. Copyright (2012) American Chemical Society.

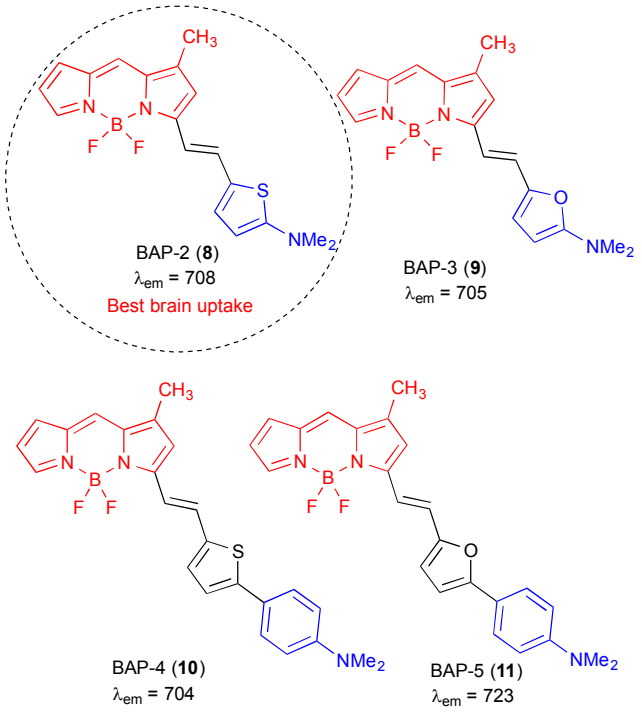

Fig. 6 BAP-1 derivatives (**8-11**) showed longer emission wavelength. Among them BAP-2 (**8**) exhibited the best uptake into and fast washout from the brain.

of transgenic mice and an age-matched control did not show a significant difference in fluorescence intensity, which was attributed to accumulation of the compound 8 in the scalp due to its affinity for lipids located in that tissue.

In the light of these findings, the conclusion emerged that, although BAP-2 possessed many features of an ideal NIR probe, further improvements were needed for its *in vivo* application.

2.2.4. AOI-987

A major achievement in the field was the generation of AOI-987 (**12**) (see its structure in Fig. 7) that allowed the visualization of β-amyloid plaques *in vivo* in a non-invasive way.[38] AOI-987 is an oxazine dye characterized by its relatively low molecular weight (427 Da) and high lipophilicity that enables the compound to cross the BBB. Due to its conjugated structure, it showed good spectral properties with both absorption and emission maximum in the NIR region, at 650 and 670 nm respectively, whereas it displayed a slight fluorescence intensity decrease instead of an enhancement of the quantum yield upon binding with Aβ aggregates. To assess the value of AOI-987 as amyloid sensor, its ability to specifically bind Aβ fibrils was evaluated *in vitro* showing a binding constant of 0.2 μM. Furthermore, compound **12** turned out to be capable of staining amyloid plaques in infected brain slices of AD mice with high selectivity. Altogether, these results suggested the application *in vivo* of AOI-987. To this end, NIR imaging was used to visualize Aβ fibrils in living APP23 transgenic mice. These mice overexpress amyloidogenic deposits that started to appear at the age of 6 months and grew with the age in terms of number and size. Following *i.v.* administration of AOI-987 (**12**) into APP23 mice, an intense fluorescence signal was detected in the brain, significantly higher than that observed in wild type mice validating the feasibility of specific plaque labeling *in vivo* (Fig. 7). Furthermore, in order to assess the ability of **12** to quantify the amyloid plaque load, transgenic mice were analysed at different disease stages showing an enhancement of the fluorescence intensity with age. It is important to note that amyloid plaques were observed without the need for any cranial windows. Afterwards, the specific labelling of Aβ was confirmed by *ex-vivo* analysis on the brain slices of the mice, which were prepared immediately after obtaining the images.

The NIR technique used to capture mice images is known as reflectance fluorescence imaging (RFI), a system that has been shown to be particularly suitable for fast imaging but has limited depth resolution beyond (3–5 mm from the surface) and is not quantitative.[15] Despite these limitations, AOI-987 was the first successful NIR probe for non-invasive *in vivo* detection of Aβ plaque formation in AD animal models. Using a NIR device, it was demonstrated that this compound was able to distinguish transgenic mice from wild type mice as well as monitor disease progression.

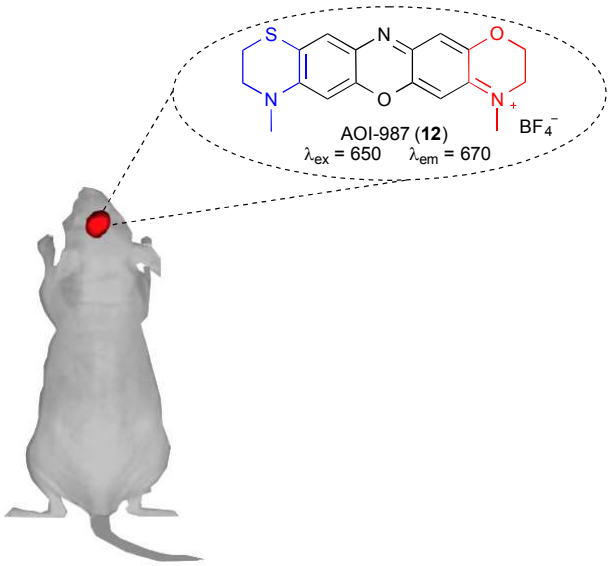

Fig. 7 AOI-987 (**12**) allowed the *in vivo* visualization of Aβ plaques in transgenic mice using NIR imaging.

2.2.5. CRANAD-2: A curcumin compound

Curcumin is the principal component of turmeric, a popular indian spice belonging to the ginger family (*Zingiberaceae*). Curcumin (see its structure in Fig. 8) has a broad spectrum of anti-inflammatory, anti-oxidant and anti-fibrilogenic activities. In addition, this natural compound has been shown to reduce both oxidative damages and Aβ plaques accumulation *in vitro* and in rat models. Nevertheless, structural modifications of curcumin are required since it induces severe diarrhea at the dosage required to reach therapeutic plasma levels in humans, it is cytotoxic to most human cell lines at 50 μM and is teratogenic for several species.

Due to its fluorescence properties, curcumin was used to image Aβ plaques *in vivo* using AD transgenic mice. It was demonstrated that curcumin crosses weakly the BBB and after 7 days of daily administration senile plaques were observed by multiphoton microscopy.[39] Although curcumin did not have ideal spectral features and the detection technique used was invasive, it was considered as a starting point to design and generate new fluorescent probes endowed with potential for imaging amyloid plaques *in vivo* by NIR imaging methods.

In this connection, Ran *et al.* reported the design, synthesis and spectroscopic evaluation for *in vivo* application of a curcumin derivative named CRANAD-2 (**13**) (Fig. 8a).[26] Compound **13** was purposely designed with the aim of pushing its emission fluorescence into an ideal NIR spectral range. The authors started their investigation from the well-known reaction between curcumin and boric acid to give rosocyanine. This compound is constituted by two curcumin moieties connected by a borate ring, which confers to its solutions a bright red colour due to the π-π* transition of a lone pair of electrons from the central oxygen to the empty orbital of boron, giving rise to an absorbance red shift. In addition, the difluoroboronate ring constitutes the central core of red-shifted bodipy dyes.[40] Thus,

it was deemed reasonable that the introduction of a difluoroboronate moiety into curcumin could provide a favourable bathochromic shift of the absorption and emission wavelength. This effect was further reinforced by replacing the phenolic hydroxyl groups of curcumin with an *N,N'*-dimethylamino group that is regarded as one of the best groups for red-shifting the absorption, leading to the design of compound **13**. This molecule had a suitably high Stokes shift and, as expected, both absorption (λ_{ex} = 640 nm) and emission (λ_{em} = 805 nm) maxima, measured in PBS, fell in the NIR region (Fig. 8a).

The affinity of **13** for synthetic Aβ aggregates was explored *in vitro*. Remarkably, the molecule "turned on" in presence of amyloid fibrils showing a significant enhancement of its fluorescent intensity (70-fold), a critical requirement for an ideal NIR sensor. On the other hand, its binding affinity to Aβ aggregates was of 38.69 nM, much higher than that of ThT and AOI-987 (**12**) and similar to that of NIAD-4 (**1**). Furthermore, the ability of CRANAD-2 to specifically detect amyloid deposits was confirmed by *in vitro* staining of AD brain slices.

In order to investigate the possibility of using CRANAD-2 for *in vivo* imaging, further experiments were carried out. It was demonstrated that **13** interacted weakly with bovine albumin, was stable in human serum and crossed the BBB *in vivo*. In view of these results, this molecular probe was injected into transgenic mice that expressed significant concentration of Aβ fibrils. Higher fluorescent signals were observed in these transgenic mice with regard of those found in control mice, confirming the feasibility of monitoring the progression of Aβ fibril formation by NIR imaging. Finally, the penetration through the BBB and the selective binding to senile plaques were confirmed by *ex vivo* histological studies on the brain sections of the sacrificed mice (Fig. 8b).

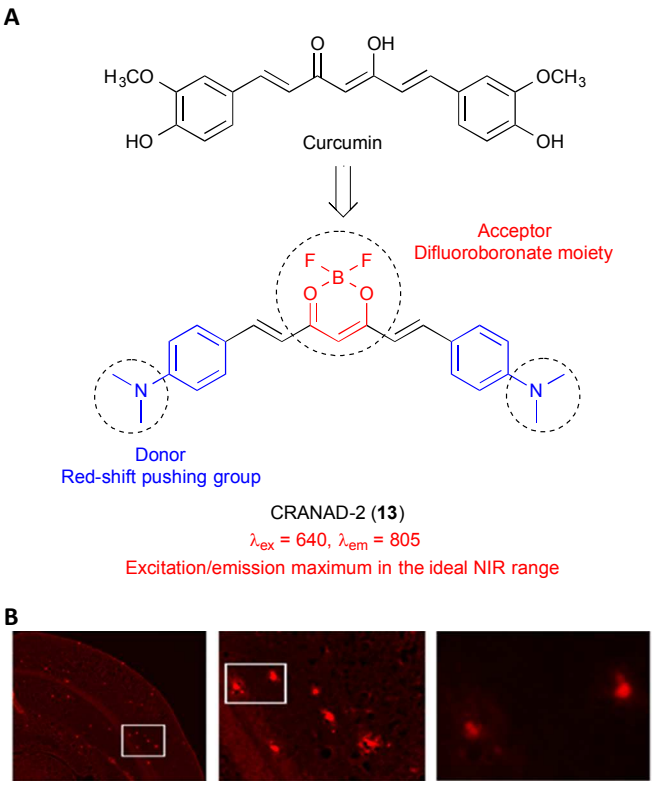

Fig. 8 (A) Chemical structure and fluorescent properties of curcumin and CRANAD-2 (**13**). This compound exhibited excitation and emission maximum in the ideal NIR spectral region. (B) Fluorescent staining with CRANAD-2 of brain sections from transgenic mice. Amplification from left to right: 2x, 10x, 40x. Reprinted (adapted) with permission from C. Ran, X. Xu, S. B. Raymond, B. J. Ferrara, K. Neal, B. J. Bacskai, Z. Medarova and A. Moore, *J. Am. Chem. Soc.* 2009, **131**, 15257. Copyright (2009) American Chemical Society.

In a nutshell, CRANAD-2 fulfilled most of the requirements for a NIR probe, and was shown to enter the brain and label specifically Aβ plaques allowing their imaging *in vivo*. Nevertheless, also in this case the NIR imaging technique employed was fluorescence reflectance, which is characterized by a low penetrating depth (< 1 cm) and a low resolution.

2.2.6. CRANAD-58

It is important to remark that during the progression of the disease, Aβ fibrils coexist with soluble Aβ species. Indeed, it is believed that the onset of AD is characterized by the excessive accumulation of soluble Aβ monomers that gradually tend to aggregate into toxic dimers and oligomers, leading to the formation of the amyloid plaques.[41,42] On this basis, Zhang *et al.* developed CRANAD-58 **14**, which has been shown to be able to detect both species of Aβ and thus offers the unique opportunity of monitoring the AD progression since its very early stage.[43]

The rational design of this compound started from the assumption that the interaction between CRANAD-2 (**13**) and Aβ fibrils takes place through a specific binding site that consists of an hydrophilic and hydrophobic segment that have been termed HHQK and LVFF. To the contrary, interaction with Aβ monomers resulted quite weak. This was due to the fact that **13** could not match the hydrophilic portion of the binding site. Since it was demonstrated that half of its molecule binds strongly to the LVFF hydrophobic segment of Aβ monomers, the other half was replaced with a similar moiety

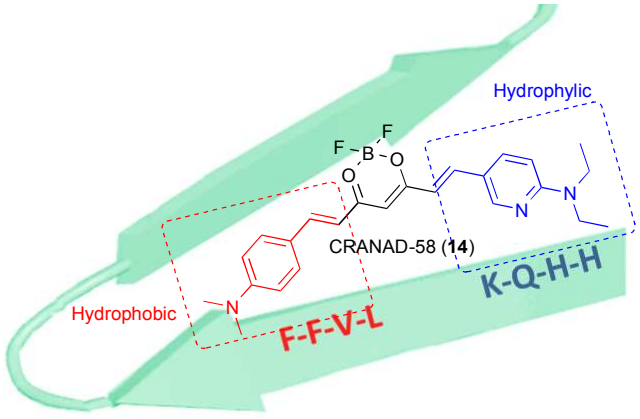

Fig. 9 CRANAD-58 (**14**) had λ_{ex} = 630 nm and λ_{em} = 750 nm and showed strong affinity to Aβ fibrils interacting specifically with its hydrophobic (FFVL) and hydrophilic (HHQK) segments that resulted in a strong enhancement of the fluorescence quantum yield.

containing a hydrophilic pyridyl ring, giving rise to the generation of CRANAD-58 (**14**), a non-symmetric curcumin analogue (Fig. 9). Compound **14** showed ideal excitation and emission peaks at 630 and 750 nm, respectively, and a dramatic enhancement of the fluorescent quantum yield was observed upon mixing Aβ soluble species including monomers, dimers, oligomers as well as fibrillar plaques. Furthermore, it has been shown to distinguish coexisting soluble and insoluble amyloid peptides due to different emission peak shifts related to the content of monomeric and aggregated Aβ species.

In order to assess its potential as an Aβ ligand in the central nervous system (CNS), compound **14** was tested *in vivo* in transgenic AD mice after having evaluated its BBB permeability. It is important to note that the APP/PS1 mice used for the experiments did not produce Aβ plaques before 6 months of age. Therefore, to study the ability of the dye to detect Aβ soluble species, 4-month old APP/PS1 mice were used. Fluorescence signals from the brains of such mice were much higher than those from wild-type mice, suggesting that monomeric Aβ species are dominant during the initial stage of AD. In the light of these findings, CRANAD-58 (**14**) was regarded to be particularly suitable for the NIR imaging and detection of Aβ soluble species, representing a feasible way to monitor AD progression since its onset. Nevertheless, current fluorescence microscopes do not have enough resolution to allow visualizing the morphology of the soluble species, and therefore it is technically not possible to validate the binding between compound **14** and the soluble Aβ peptides *in vivo* and *ex vivo*.

2.2.7. THK

An important breakthrough in the search for novel NIR probes to be used *in vivo* was achieved with the discovery of THK-265 (**15**).[44] This compound was identified through a virtual screening of NIR candidates and has the advantage of being commercially available.

Compound **15** is formed by two thiobarbituric acid units connected by a pentadienylidene chain, forming an extended conjugated system after oxo-enol tautomerism at one of the lactam groups. It showed suitable spectroscopic properties, with an emission maximum at $\lambda > 650$ nm and a high fluorescent quantum yield (38.5% in methanol). Importantly, a fluorescent binding assay revealed a strong affinity to Aβ aggregates, higher than that of ThT and AOI-1987 (**12**), which was confirmed by a fluorescent staining on AD brain slices, and showing an enhanced fluorescence intensity upon binding to fibrils. Since the dye **15** also exhibited a low toxicity and a good brain uptake, its capability of visualizing Aβ plaques was explored *in vivo*. Thus, the compound was intravenously injected into AβPP-transgenic mice that overexpressed senile plaques and the fluorescent signal intensity observed was significantly higher than that detected in wild type mice. It is important to note that the discrimination between the specific probe accumulation in transgenic mice and the nonspecific probe accumulation in control mice was achieved almost immediately after the injection of **15**, whereas in the case of AOI-1987 (compound **12**) a quite long time was required to observe differences between the two types of mice. Again, all the results obtained *in vivo* were validated *ex vivo*, confirming the ability of this compound to cross the BBB and selectively label Aβ plaques.

In the light of these findings, Schmidt *et al.* developed a systematic protocol to image and quantify amyloid fibrils in transgenic mice at different disease stages using THK-265 as NIR probe.[45] All the experiments were carried out involving AβPP-transgenic mice that started to show senile plaques after 50 days. Considering that the number and size of the Aβ plaques increased with age, the mice were scanned at different ages: 50, 75, 100 and older than 200 days in order to monitor the amyloid accumulation. Importantly, *in vivo* results confirmed a direct correlation between the enhancement of the fluorescence intensity signal and the increasing age of the mice (Fig.10b). As expected, *ex vivo* experiments proved that fluorescent signal changes were due to the different Aβ loads. Nevertheless, higher sensitivity is needed to real-time monitor cerebral amyloid deposits by using NIR imaging, even if THK-265 could represent a possible candidate to track AD progression and evaluate the efficacy of anti-AD drug.

2.2.8. DANIRs

Although all the NIR probes for Aβ imaging discussed so far are able to cross the BBB and label selectively the amyloid plaques, they still show limitations that need to be overcome. For example, NIAD-4 (**1**) could not be detected in mice with an intact cranium, BODIPY7 (**6**) and BAP-1 (**7**) exhibited poor BBB permeation, AOI-1987 (**12**) showed only moderate affinity for Aβ aggregates and CRANAD-2 (**13**) displayed a

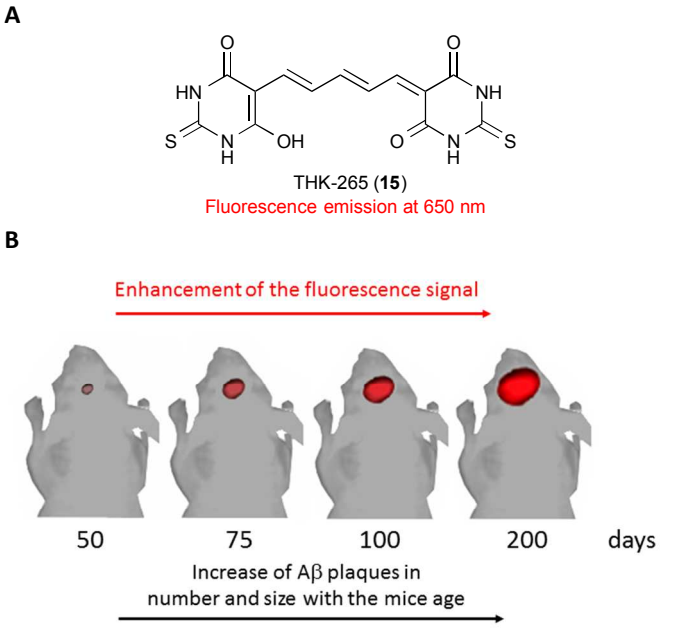

Fig. 10 (A) Chemical structure of THK (**15**). (B) The fluorescence intensity signal of THK enhances with the increasing age of the mice.

low washout from the brain. In an effort to design improved NIR probes, Cui et al. developed a new series of fluorescent small molecules for *in vivo* detection of Aβ plaques.[46] The authors used the push-pull architecture to generate new compounds that consisted of a donor and acceptor connected by a conjugated π electron chain. The N,N'-dimethylamino group was selected as the electron donor because of its known ability to redshift light absorption, and a dicyanomethylene group was chosen as acceptor. The donor-acceptor system was separated by a polymethine moiety that was expected to further push both absorption and emission wavelength toward the NIR spectral region. In this regard, different lengths of the conjugated chain were explored, leading to the generation of three compounds that the authors designed as DANIRs (compounds **16-18**, Fig. 11a). As expected, a native fluorescent study performed in PBS revealed that the molecule with the longer chain, compound **18**, showed the most red-shifted emission wavelength at 665 nm. This behaviour was due to the fact that an extended conjugated system reduces the energy gap between HOMO and LUMO, resulting in a significant bathochromic shift on the emission wavelength. Such effect is further reinforced by the fact that the whole structure is approximately planar.

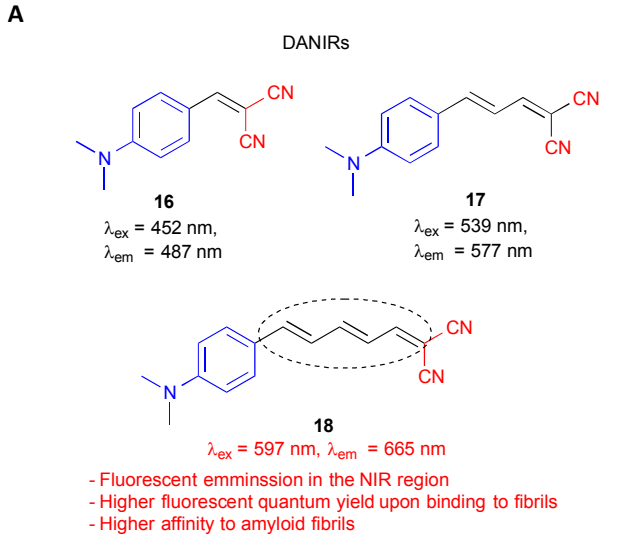

Fig. 11 (A) Chemical structure and optical properties of compounds **16-18**. Due to its favourable florescent features and high affinity to amyloid fibrils, **18** was selected for *in vivo* NIR imaging. (B) Fluorescence staining with **18** of a brain section from a transgenic mouse compared with that from a wild type one. Reprinted (adapted) with permission from M. Cui, M. Ono, H. Watanabe, H. Kimura, B. Liu and H. Saji, *J. Am. Chem. Soc.*, 2014, **136**, 3388. Copyright (2014) American Chemical Society.

In order to establish the application of these molecules as Aβ sensors, a series of *in vitro* experiments were carried out. First, their binding affinities to Aβ aggregates were evaluated. The results showed that compound **18** possessed the highest affinity to amyloid fibrils, displaying an inhibition constant (K_i) of 36.9 nm, showing that the length of the conjugated bridge plays a critical role for Aβ binding. The specific labelling to senile plaques was confirmed by an *in vitro* neuropathological fluorescence staining on brain slice from AD patients and APP transgenic mice.

Another important feature of a NIR probe is its ability to increase the fluorescence intensity upon binding to Aβ aggregates. Interestingly, compound **18** showed a significant enhancement of the fluorescent quantum yield (12-fold) upon association with the fibrils. It is interesting to note that this molecule showed low toxicity, good stability in human serum and weak interactions with bovine serum albumin (BSA). Due to all these favourable properties, compound **18** was selected for *in vivo* experiments to prove its potential to visualize Aβ plaques *in vivo* using NIR imaging. First, the NIR imaging was carried out on the normal mice to study the biodistribution and brain kinetics of **18**. The data demonstrated that it was able to cross the BBB and could be quickly washed out from the brain. Thus, following administration of **18** to APPswe/PSEN1 double transgenic mice, the fluorescent signal detected was remarkably higher than that for the wild-type control. Importantly, this specific labelling was confirmed *ex vivo* (Fig. 11b). Taken in the aggregate, these results confirmed that compound **18** meets the requirements for an ideal NIR probe.

3. Theranostics

As discussed in the introduction, the amyloid aggregates have been historically considered as the *post-mortem* neuropathological hallmarks of AD and, more recently, the proper biomarker for clinical diagnosis. At the same time, amyloid aggregates have been viewed as a potential therapeutic target for drug discovery, and tremendous effort has been expended in the last years on developing new molecules capable of inhibiting Aβ aggregation.[47] These considerations open the possibility to develop fluorescent probes able to detect amyloid deposition and, at the same time, provide therapeutic strategies. In other words, such molecules could act as theranostics.[4] This neologism emphasizes the ability of a properly designed agent to integrate imaging and therapeutic functions in a single platform. Despite the fact that research in this field is just at its beginning, several examples of nanoparticles for improving diagnosis and therapy of AD have already been reported.[48]. In parallel to nanoparticles, the possibility of developing theranostic small molecules was recently explored by us *via* the generation of a library of styrylquinoline derivatives and the investigation of their profile in terms of therapeutic and diagnostic properties against two PMD such as AD and prion diseases.[49] It is interesting to note that quinoline compounds were also identified as candidates for tau imaging tracer.[50]

The synthesized styrylquinoline derivatives exhibited a promising activity against prion replication in ScGT1 cell model, while showing no appreciable cytotoxicity. In particular (*E*)-6-methyl-4-amino-2-styryl-quinoline G8 (**19**) displayed a remarkable submicromolar activity ($EC_{50} = 0.5 \pm 0.1$ μM). We also verified its activity as an inhibitor of Aβ and PrP^{Sc} aggregation *in vitro*. In addition, we could predict the ability of **19** to cross the BBB in a parallel artificial membrane permeation assay for the BBB (PAMPA-BBB). To corroborate the possibility of employing this compound as a useful NIR amyloid-binding probe, we investigated its native fluorescence in a variety of polar and non-polar environments modeling its interaction with proteins. Interestingly, we noted that the fluorescent spectra of the hydrochloride form of **19**, in its solid state, showed an emission maximum above 600 nm (NIR region). As another positive feature, **19** significantly changed its fluorescence properties upon binding to Aβ aggregates, while having weak interactions with BSA. To confirm the labeling of amyloid aggregates in living cells, fluorescent staining with G8 was carried out using the same ScGT1 cell model. We found that 0.025% of G8·HCl (0.84 mM) was sufficient to observe many fluorescent spots in the treated cells examined with a fluorescence microscopy using a ThS filter set (within the NIR optical window). Importantly, no spots were observed in the uninfected cells, confirming a specific binding to amyloid protein. In summary, G8 represents a promising starting point for further improvement in terms of activity and bioimaging for a possible application *in vivo*.

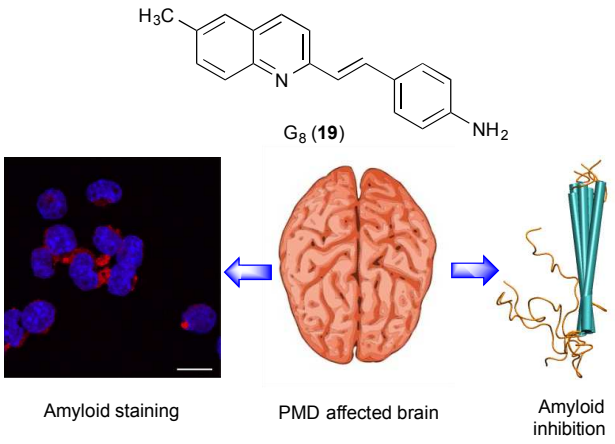

Fig. 12 The integrated therapeutic and diagnostic features of G8 (**19**). It detects amyloid aggregates and inhibits amyloid aggregation with no apparent toxicity.

4. Conclusions

In the last decade several progresses have been done in the field of bioimaging using non-invasive fluorescent NIR probes. In this review we report a series of molecules that turned out to be able to image Aβ plaques *in vivo* in animal models, highlighting the improvements that have been achieved since the discovery of the first NIR sensor that required a cranial window to be detected until the generation of smart probes capable of real-time monitoring the progress of AD in transgenic mice with intact cranium. Furthermore, with the multi-modal fluorescence imaging, it would be feasible to track biomarkers at depths up to 3–5 cm, which should be sufficient to diagnose and monitor AD progression. Particular attention was given to the molecular design of the probes to red-shift their fluorescent emission toward the NIR spectral region and all the structural modifications of existing NIR dyes to improve their photophysical and photochemical properties were described. In addition, we outlined the high importance of NIR imaging as a versatile and sensitive method for studying the potential effectiveness of anti-AD drug candidates in small animals, since PET is not ideal for this purpose. Nevertheless, despite the favourable features of the reported NIR probes for their *in vivo* application and the great strides forward that have been made, their translation into the clinical practice remains challenging and further optical improvements and technological evolutions are needed.

Acknowledgements

Financial support from Ministerio de Economía y Competitividad, MINECO (grant CTQ2012-33272-BQU) and Universidad Complutense (grant GR35/10-A-920234 and fellowship to M.S.) is gratefully acknowledged. MLB and MS also acknowledge the support of EU-COST Action TD1004.

Notes and references

[a] Departamento de Química Orgánica y Farmacéutica, Facultad de Farmacia, Universidad Complutense, 28040 Madrid, Spain. Phone: +34-913-941-840; fax: +34-913-941-822; e-mail: josecm@farm.ucm.es (J. C. Menéndez)

[b] Departamento de Química Analítica, Facultad de Farmacia, Universidad Complutense, 28040 Madrid, Spain

[c] Dipartimento di Farmacia e Biotecnologie, Alma Mater Studiorum University of Bologna, Via Belmeloro 6, 40126 Bologna, Italy

1 F. Chiti, C. M. Dobson, *Annu. Rev. Biochem.,* 2006, **75**, 333.
2 L. Mucke and D. J. Selkoe, *Cold Spring Harb. Perspect. Med.*, 2012, **2**, a006338.
3 M. Jucker, *Nature Medicine,* 2010, **16**, 1210.
4 M. L. Bolognesi, 2013, in Lackey K, Roth BD (Ed.), Medicinal Chemistry Approaches to Personalized Medicine, Chapter 9. Wiley-VCH, 2013.
5 C. W. Bertoncini, M. S. Celej, *Curr. Protein Pept. Sci*., 2011, **12**, 206.
6 S. B. Raymond, A. T. Kumar, D. A. Boas and B. J. Bacskai*, Phys. Med. Biol.*, 2009, **54**, 6201.
7 G. Hong, S. Diao, J. Chang, A. L. Antaris, C. Chen, B. Zhang, S. Zhao, D. N. Atochin, P. L. Huang, K. I. Andreasson, C. J. Kuo and H. Dai, *Nat. Photon*., 2014, **8**, 723.
8 T. K. Khan, D. L. Alkon, *Neurobiol. Aging*, 2010, **31**, 889.
9 J. O. Escobedo, O. Rusin, S. Lim and R. M. Strongin, *Curr. Opin. Chem. Biol.*, 2010, **14**, 64.
10 K. Kiyose, H. Kojima and T. Nagano, *Chem. Asian J*., 2008, **3**, 506.
11 S. A. Hilderbrand and R. Weissleder, *Curr. Opin. Chem. Biol.,* 2010, **14**, 71.
12 G. Qian and Z. Y. Wang, *Chem. Asian J.*, 2010, **5**, 1006.

13 Z. Guo, S. Park, J. Yoon and I. Shin, *Chem. Soc. Rev.,* 2014, **43**, 16.
14 L. Yuan, W. Lin, K. Zheng, L. He and W. Huang, *Chem. Soc. Rev.*, 2013, **42**, 622.
15 V. Ntziachristos, *Nature Methods,* 2010, **7**, 603.
16 M. T. Fodero-Tavoletti, C. C. Rowe, C. A. McLean, L. Leone, Q. X. Li, C. L. Masters, R. Cappai and V. L. Villemagne, *J. Nucl. Med.*, 2009, **50**, 198.
17 Y. Koronyo, B. C. Salumbides, K. L. Black, M. Koronyo-Hamaoui, *Neurodegener. Dis.*, 2012, **10**, 285.
18 C. Schon, N. A. Hoffmann, S. M. Ochs, S. Burgold, S. Filser, S. Steinbach, M. W. Seeliger, T. Arzberger, M. Goedert, H. A. Kretzschmar, B. Schmidt, J. Herms, *Plos One*, 2012, **7**, e53547.
19 J. Gu, U. R. Anumala, R. Heyny-von Haußen, J. Hölzer, V. Goetschy-Meyer, G. Mall, I. Hilger, C. Czech, B. Schmidt, *ChemMedChem*, 2013, **8**, 891.
20 S. S. Kelkar and T. M. Reineke*, Bioconjug. Chem.* 2011, **22**, 1879.
21 T. Lammers, S. Aime, W. E. Hennink, G. Storm and F. Kiessling, *Acc. Chem. Res.,* 2011, **44**, 1029.
22 S. Gupta, P. Babu and A. Surolia, *Biomaterials*, 2010, **31**, 6809.
23 For a review of the toxicological effects of NPs and quantum dots, see: R. Hardman, *Environ. Health Persp*., 2006, **114**, 165.
24 Q. Li, J. S. Lee, C. Ha, C. B. Park, G. Yang, W. B. Gan and Y. T. Chang, *Angew. Chem. Int. Ed.,* 2004, **43**, 6331.
25 E. E. Nesterov, J. Skoch, B. T. Hyman, W. E. Klunk, B. J. Bacskai, T. M. and Swager, *Angew. Chem. Int. Ed.* 2005, **44**, 5452.
26 C. Ran, X. Xu, S. B. Raymond, B. J. Ferrara, K. Neal, B. J. Bacskai, Z. Medarova and A. Moore, *J. Am. Chem. Soc.,* 2009, **131**, 15257.
27 L. Yuan, W. Lin, S. Zhao, W. Gao, B. Chen, L. He and S. Zhu, *J. Am. Chem. Soc.,* 2012, **134**, 13510.
28 S. Yao, H. Y. Ahn, X. Wang, J. Fu, E. W. Van Stryland, D. J. Hagan and K. D. Belfield, *J. Org. Chem.*, 2010, **75**, 3965.
29 J. Dong, R. Revilla-Sánchez, S. Moss and P. G. Haydon, *Neuropharmacology*, 2010, **59**, 268.
30 A. I. Sulatskaya, A. A. Maskevich, I. M. Kuznetsova, V. N. Uversky, K. K. Turoverov, *Plos One*, 2010, **5**, e15385.
31 S. B. Raymond, J. Skoch, I. D. Hills, E. E. Nesterov, T. M. Swager and B. J. Bacskai, *Eur. J. Nucl. Med. Mol. Imaging*, 2008, **35**, S93.
32 W. E. Klunk, B. J. Bacskai, C. A. Mathis, S. T. Kajdasz, M. E. McLellan, M. P. Frosch, M. L. Debnath, D. P. Holt, Y. Wang, B. T. Hyman, *J. Neuropathol. Exp. Neurol.*, 2002, **61**, 797.
33 K. P. Nilsson, P. Hammarström, F. Ahlgren, A. Herland, E. A. Schnell, M. Lindgren, G. T. Westermark, O. Inganäs, *Chembiochem.*, 2006, **7**, 1096.
34 A. Ojida, T. Sakamoto, M. A. Inoue, S. H. Fujishima, G. Lippens and I. Hamachi, *J. Am. Chem. Soc.*, 2009, **131**, 6543.
35 M. Ono, M. Ishikawa, H. Kimura, S. Hayashi, K. Matsumura, H. Watanabe, Y. Shimizu, Y. Cheng, M. Cui, H. Kawashima and H. Saji, *Bioorg. Med. Chem. Lett.*, 2010, **20**, 3885.
36 M. Ono, H. Watanabe, H. Kimura and H. Saji, *ACS Chem. Neurosci.*, 2012, **3**, 319.
37 H. Watanabe, M. Ono, K. Matsumura, M. Yoshimura, H. Kimuraand, H. Saji, *Mol. Imaging*., 2013, **12**, 338.
38 M. Hintersteiner, A. Enz, P. Frey, A. L. Jaton, W. Kinzy, R. Kneuer, U. Neumann, M. Rudin, M. Staufenbiel, M. Stoeckli, K. H. Wiederhold and H. U. Gremlich, *Nat. Biotechnol.,* 2005, **23**, 577.
39 M. Garcia-Alloza, L. A. Borrelli, A. Rozkalne, B. T. Hyman and B. J. Bacskai, *J. Neurochem.*, 2007, **102**, 1095.
40 G. Ulrich, R. Ziessel, A. Harriman, *Angew. Chem. Int. Ed. Engl.,* 2008, **47**, 1184.
41 J. Hardy, D. J. Selkoe, *Science*, 2002, **297**, 353.
42 M. N. Pangalos, L. E. Schechter and O. Hurko, *Nat. Rev. Drug Discov.,* 2007, **6**, 521.
43 X. Zhang, Y. Tian, Z. Li, Tian X, H. Sun, H. Liu, A. Moore and C. Ran, *J. Am. Chem. Soc.*, 2013, **135**, 16397.
44 N. Okamura, M. Mori, S. Furumoto, T. Yoshikawa, R. Harada, S. Ito, Y. Fujikawa, H. Arai, K. Yanai and Y. Kudo, *J. Alzheimers Dis.*, 2011, **23**, 37.
45 A. Schmidt and J. Pahnke, *J. Alzheimers Dis.*, 2012, **30**, 651.
46 M. Cui, M. Ono, H. Watanabe, H. Kimura, B. Liu and H. Saji, *J. Am. Chem. Soc.,* 2014, **136**, 3388.
47 C. I Stains, K. Mondal and I. Ghosh, *ChemMedChem*., 2007, **2**, 1674.
48 K. Andrieux and P. Couvreur, *Ann. Pharm. Fr.,* 2013, **71**, 225.
49 M. Staderini, S. Aulić, M. Bartolini, H. N. Ai Tran, V. González-Ruiz, D. I. Pérez, N. Cabezas, A. Martínez, M. A. Martín, V. Andrisano, G. Legname, J. C. Menéndez and M. L. Bolognesi, *ACS Med. Chem. Lett.,* 2013, **4**, 225.
50 V. L. Villemagne, N. Okamura, *Alzheimers Dement.*, 2014, **10**, S254-64

